Bioorganic Chemistry 127 (2022) 105927

Contents lists available at ScienceDirect

Bioorganic Chemistry

journal homepage: www.elsevier.com/locate/bioorg

Nanotechnology applications for treatment of hepatic infections via modulating Hepatic histopathological and DNA alterations

Sameh S. Gad [a], Dina S. Abdelrahim [b], Sameh H. Ismail [c], Sherine M. Ibrahim [d,*]

[a] Department of Pharmacology, Faculty of Pharmacy, October University for Modern Sciences and Arts (MSA), Giza, Egypt
[b] Department of Pharmacology, Faculty of Medicine, Cairo University, Giza, Egypt
[c] Department of Pharmacology, Faculty of Nanotechnology for postgraduate studies, Cairo University, Sheikh Zayed Branch Campus, Sheikh Zayed City, Egypt
[d] Biochemistry Department, Faculty of Pharmacy, October University for Modern Sciences and Arts (MSA), Giza, Egypt

ARTICLE INFO

Keywords:
Silver nanoparticles
Selenium nanoparticles
Oxidative stress
hepatitis B virus
Interleukin-6
Tumor necrosis factor -α

ABSTRACT

Background: Nanoparticles are recently playing a potential role in improving drug uptake and the treatment of diseases. A variety of nanoparticles, such as selenium nanoparticles (SeNPs) and Silver nanoparticles (AgNPs) have been used as drug carriers in various ways for treatment of cancers and liver diseases. Our aim in this study is to investigate the ability of AgNPs and SeNPs to target and treat the viral and bacterial infection of liver in rats and cell lines.

Methods: For assessment of antioxidant activity of silver nanoparticles, six adult male albino rats were included in this study, liver slices were taken and assigned to 6 groups. Markers of hepatic functions, oxidative stress and inflammation in liver slices are carried out. While for assessment of antiviral activity of SeNPs, HBV-replicating human cell line HepG2 and normal human cell lines were used, hepatic and inflammatory alterations are determined through quantitative polymerase chain reaction (PCR) and comet assay techniques.

Results: The effect of Ag-NPs on interleukin-6 (IL-6) and tumor necrosis factor (TNF-α) levels were reduced in different treated groups with Ag-NPs compared with the control and diseased groups. On the other hand, SeNPs revealed significant alterations in the inflammatory markers as well as DNA damage in the treated HBV- human cell line HepG2 compared to the diseased ones.

Conclusion: Silver nanoparticles have the ability for producing various hepatic alterations and can inhibit the proliferation of hepatic stellate cells (HSCs) in a dose and size dependent manner. On the other hand, SeNPs showed excellent selectivity towards viral cells in the HepG2 cell lines. Both Ag-NPs and SeNPs might be a promising drug design for treating viral and bacterial liver diseases.

1. Introduction

Nanoparticles have been widely investigated over the past decades, due to their special physical and chemical properties. The main properties of nanomaterials depend mainly on their morphology and particle size. AgNPs and SeNPs are the most commercialized nanoparticles used in medical researches for medical applications such as gene, antimicrobial agents and drug delivery carriers [1].

AgNPs have been shown to significantly cure chronic liver diseases [2]. Additionally, these AgNPs have been used to target specific injured tissues in blood circulation through the combination of antibody-based targeting of ligands and material composition. Ag ions in sufficient concentration readily kills bacteria in vitro. These studies showed the potential effect of AgNPs for the cure of liver diseases including bacterial infection and hepatic fibrosis [3].

Recently, traditional chemotherapy and anti-fibrotic treatments became ineffective in treatment of chronic liver diseases, due to the development of resistant drug tolerance. Thus, AgNPs may provide a safer therapeutic tool of treatment for targeting the hepatic stellate cells (HSCs), which are the main focus for treatment of liver cirrhosis and

Abbreviations: AST, Aspartate transaminase; ALT, Alanine transaminase; ELISA, Enzyme-linked immunosorbent assay; GSH, Glutathione; HSC s, Hepatic stellate cells; HBV, Hepatitis B virus; IL-8, Interleukin -8; MDA, Malondialdehyde; NOS, Nitric oxide reactive species; AgNPs, Sliver nanoparticles; SeNPs, Selenium nanoparticles; ROS, Reactive oxygen species; TBARS, Thiobarbituric acid reactive substances; TSC, Trisodium citrate; TNF-α, Tumor necrosis factor; TGF, Tumor growth factor; PCR, Polymerase chain reaction.

* Corresponding author.
E-mail address: sherinemahmoud@msa.edu.eg (S.M. Ibrahim).

https://doi.org/10.1016/j.bioorg.2022.105927
Received 30 September 2021; Accepted 1 June 2022
Available online 17 June 2022

hepatic fibrosis [4].

SeNPs are regarded recently as new nanoparticles and have shown great interest due to their higher anti-inflammatory, antiviral and anti-tumor activity, lower-toxicity to normal cells compared with other used nanoparticles [5]. Taken into consideration, selenium (Se) is an essential element which has many important functions in the human body including protection of the cardiovascular and liver organs, regulation of secretion of hormones, and free radical scavenger. Recent studies have shown that SeNPs has potential therapeutic action for treatment of many diseases including inflammation, virus infection, and cancer [6]. This new nanoparticle provides a promising tool for treatment of many liver diseases [7].

In this study, we will investigate the efficiency of AgNPs in treatment of liver bacterial infection in rats and the efficiency of SeNPs for targeting and treatment of HBV infected cell lines by evaluating their hepatic and inflammatory changes.

2. Materials and methods

2.1. Preparation and synthesis of AgNPs

Two sizes of silver nanoparticles were purchased from (Egypt Center for nanotechnology), as small particle size (10 nm and 75 nm) and large particle size (250–300 nm). The size, morphology and dispersion of the nanoparticles were characterized using a Tecnai™ G2 Twin Transmission Electron Microscope (FEI, Hillsboro, OR, USA) and dynamic light scattering (Compact Goniometer System 3; ALV-GmbH, Langen, Germany). Synthesis of silver nanoparticles was achieved by precipitation method using trisodium citrate (TSC) as reducing agent and capping one in the same time. AgNO3 solution (0.03 M) was dissolved in 200 ml deionized water, heated to boiling, then 0.3 M TSC was added drop by drop with slowly stirring and heated until the color of solution become pale yellow. The final solution was cooled at room temperature in isolated dark area to avoid lights [8].

2.1.1. Experimental animal design and conditions

Six adult male albino rats weighing from 200 to 250 g were used. Rats were housed at MSA animal house under standard laboratory conditions and suitable temperature. They were housed in plastic cages, given standard normal diet and water. The work was done according to ethical committee guidelines in faculty of pharmacy and animal experimentations guideline at MSA University (**code: PH8/EC8/2019F**). After reaching to target weight (250 gm), animals were sacrificed to take their livers.

The livers were immediately freezed then kept in fridge for 24 h. Then, according to Olinga and Sshuppan (2016), a precision cut liver slices was carried out using Cryostat macrotome device in Animal health research institute, the thickness of the slice was optimized to 150 μm. The freshly liver slices (14 slice each 150 μm thickness) are transferred to six well plate under controlled physiological conditions. We used six well plate and distribute the slices evenly, every well contained two slices exactly. So, all the wells contain the same weight and characti-zation. The six well plate were assigned to group 1: (Normal) containing Ringer solution only, group 2: (control) lipopolysaccharide (LPS) 0.5 ml of (5 mg/ 13 ml distilled water) + Ringer solution, group 3: LPS + *N*-acetylcysteine (NAC) + Ringer solution, group 4: (standard treatment) LPS 0.5 ml of (5 mg/ 13 ml distilled water) + AgNpS(1–100 nm) + Ringer solution, group 5: (treatment I) LPS 0.5 ml of (5 mg/ 13 ml distilled water) + AgNpL 0.5 ml (150–300 nm) + 2 ml Ringer solution and group 6: LPS 0.5 ml of (5 mg/ 13 ml distilled water) + NAC + AgNpS (1–100 nm) 0.5 ml + 2 ml Ringer solution, Group 7: LPS 0.5 ml of (5 mg/ 13 ml distilled water) + NAC + AgNpL (150–300 nm) 0.5 ml + 2 ml Ringer solution. In all wells the ringer solution was added equally; The plates were then incubated in a humidified incubator in research lab at MSA University under conditions of 95% oxygen and 5% carbon dioxide to maintain slices viability. After 24-hour incubation, plates were gently removed and the supernatant and tissue homogenate were all collected and then subjected for analysis. Same steps were repeated six times with each rat n = 6.

2.1.2. Hepatic function tests analysis

Serum aspartate aminotransferase (AST) and alanine aminotransferase (ALT) were assayed in liver slices using (Biodiagnostics, CA, USA).

2.1.3. Oxidative stress analysis

GSH assay: Liver slices were kept frozen at − 20 ∘C and tissue homogenate was made in glass homogenizer using 5% 5-suphosalicylic acid for (GSH). GSH level was assayed using the dithio-binitrobenzoic acid method [9].

2.1.4. Cytokine detection

The quantity of anti- inflammatory markers; IL-6 and TNF-α, in the liver slices homogenate -conditioned medium was quantified using an enzyme-linked immunosorbent assay (ELISA) kit (MyBiosource, Inc., San Diego., USA.) according to the manufacturer's instructions.

2.1.5. Histopathological and immunohistochemistry assessment

After fixation of liver specimens in 10% formaldehyde in PBS, liver slices were then dehydrated, embedded into paraffin and sections were made at a thickness of 5 μm. These sections were carefully stained with hematoxylin and eosin (H&E) for histopathology [10]. Briefly, liver tissue sections were cut into 5 μm sections and subjected to deparaffinization and heat-induced antigen then endogenous peroxidase and protein blocking steps. After washing, liver tissue sections were incubated with primary antibodies (anti-CD68, Santa Cruz Biotechnology Inc.) overnight at 4 °C with a dilution ratio of 1:200 in PBS. HRP-labelled secondary antibodies (Abcam, UK) was applied for 2 h after washing. Finally, DAB-substrate kit was then used for color development and Meyers hematoxylin was used as counter stain.

2.2. Preparation of selenium nanoparticles (Se-NPs)

Synthesis of Se-NPs have been done by precipitation – sono-chemical method using ascorbic acid and TSC as reducing- capping agent in the same time. Na_2SeO_3 solution (0.1 M) was dissolved in 120 ml of doubled deionized water until the solution become colorless using ultrasound instrument Hielscher $400UP_S$, Germany at amplitude of 74% for 1 min at temperature of 45°c. Then a mixture of ascorbic acid and TSC (0.2 M to 0.1 M for ascorbic acid and TSC, respectively.) are added drop by drop until the color of mixture become pale brown. The solution was cooled at room temperature in dark condition [11].

2.2.1. HBV infection and DNA analysis

HBV-replicating human HCC cell line HepG2. Were maintained in Dulbecco's Modified Eagle's Medium supplemented with 10% fetal bovine serum. Cell lines were cultured at 37 °C in a humidified chamber supplemented with 5% CO2. One group left as control and 2 groups were infected by HBV-positive sera.

Cells were incubated with HBV-positive sera (10^9 particles/ml) for 14 h at 37 °C, washed extensively with PBS and fresh medium was added. For PCR analysis, at 4 days post-infection cells were washed extensively in PBS, collected using a rubber policeman and lysed in a proteinase K lysis buffer for 6 h at 37 °C, extracted with phenol–-chloroform and precipitated with ethanol. The amount of DNA was determined by conducting semi-quantitative PCR analysis of HBsAg using (Brilliant II-PCR Master Mix Kit, 1-Step, Agilent, CA, USA).

2.2.2. Determination of hepatic function tests and oxidative stress marker

The cell culture media from each of the 25 cm2 culture flasks was collected, centrifuged at 3000 × g for 10 min and stored at −70 °C until assay. ALT and AST were assayed using (Biodiagnostics, CA, USA) while MDA was determined by thiobarbituric acid reactive substances

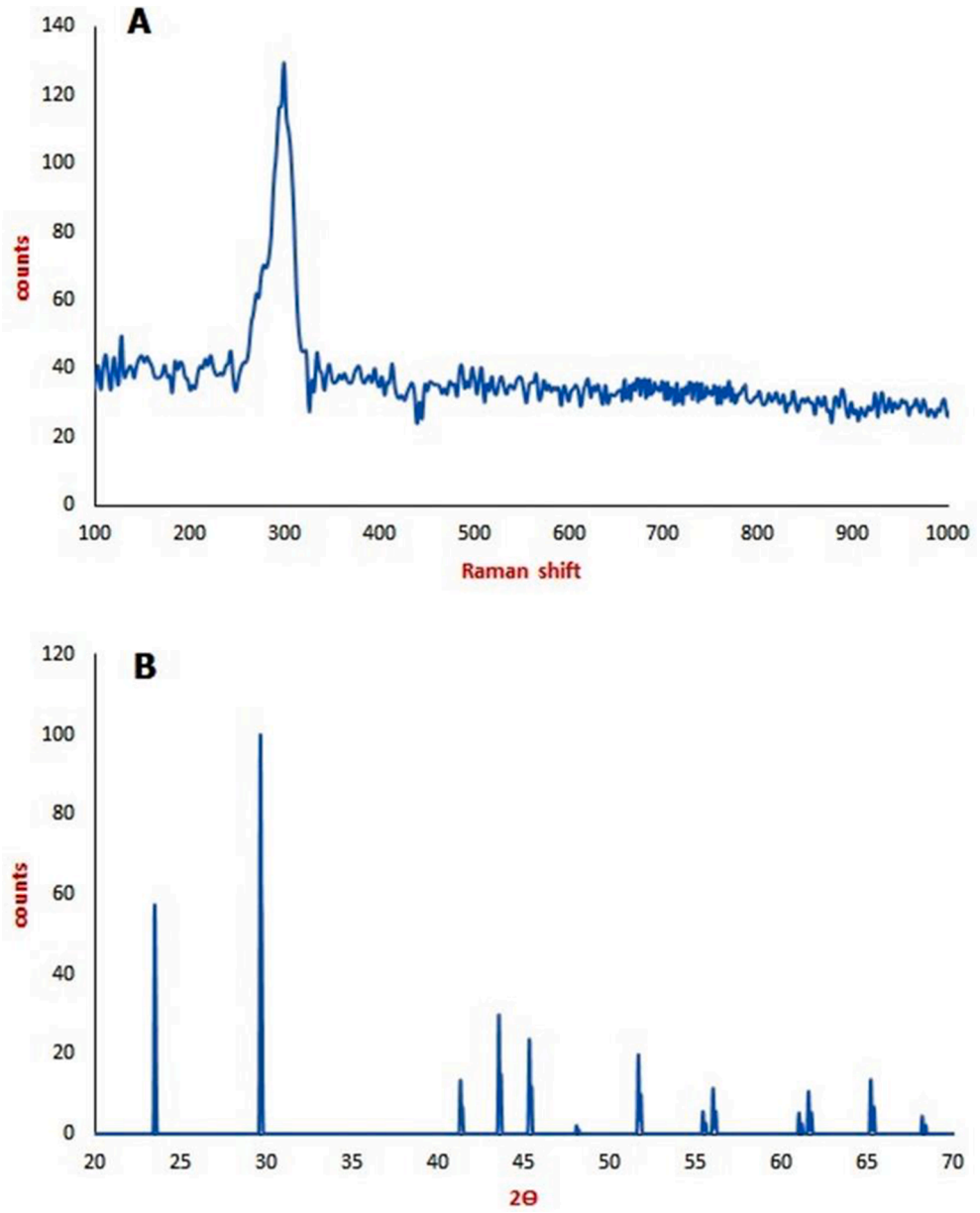

Fig. 1. (A) Raman spectrum of colloidal Se-NPs showing no contaminated peaks with a very strong sharp peaks at 300 cm-1 and (B) X-ray Diffraction (XRD) pattern of Se-NPs showed the characteristic peaks for Se-NPs at 2θ, 23.5°, 29.6°, 41.3°, 43.5°, 45.3°, 48.2°, 51.7°, 56°, 56.1°, 61°, 61.2°, 65.2°, 68.2 and 68.4°.

(TBARS) method [12].

2.2.3. Cytokine detection

IL-2 was determined using IL-2 ELISA Kit (ab46032) and IL-8 was measured using IL-8 (CXCL8) ELISA Kit for cell culture supernatants by following the kit protocol while TNF-α was assayed by following the ELISA kit protocol (Cat: KIT10602) and TGF was measured using TGF -α Human (ab100647).

2.2.4. Quantification of HBV genomic DNA by real time PCR

HBV genomic DNA extraction and sequencing analyses. HBV genomic DNA was extracted from the supernatants of co-cultured HepG2 cells using a Viral DNA Isolation Kit (Qiagen, germany) following the manufacturer's instructions. Briefly, cell supernatants were added to virus lysis buffer, and the lysates were loaded onto the spin column. After viral DNA was bound to the membrane, the column was washed and finally, the viral DNA was eluted. PCR was performed using HBV genomic DNA as template to amplify the X gene primer and probe sequences are as follows: forward primer HBV-F3, 5′-GGCCAT-CAGCGCATGC-3′, and reverse primer HBV-R3M3, 5′-C [5-NitIdl] GCTGCGAGCAAAACA-3′; and probe HBV-*P*3, 5′-R-CTCTGCCGATCCA-TACTGCGGAACTC-Q-3. The PCR conditions were: initial denaturation at 94 °C for 2 min, followed by 35 cycles of 94 °C for 30 s, 55 °C for 30 s, and 72 °C for 1 min, and a final extension was performed at 72 °C for 10 min.

2.2.5. Comet assay

The extent of DNA damage was accessed using the comet assay under alkaline conditions. Comet tail length was measured by fluorescence microscopy and then analyzed using CaspLab Comet Assay Software v1.2.3 (Tritek Corporation, Summerduck, VA).

2.3. Characterization of silver nanoparticles and selenium nanoparticles

2.3.1. Identification class

X-ray Diffraction (XRD) Bruker D8 Discover device was used for XRD

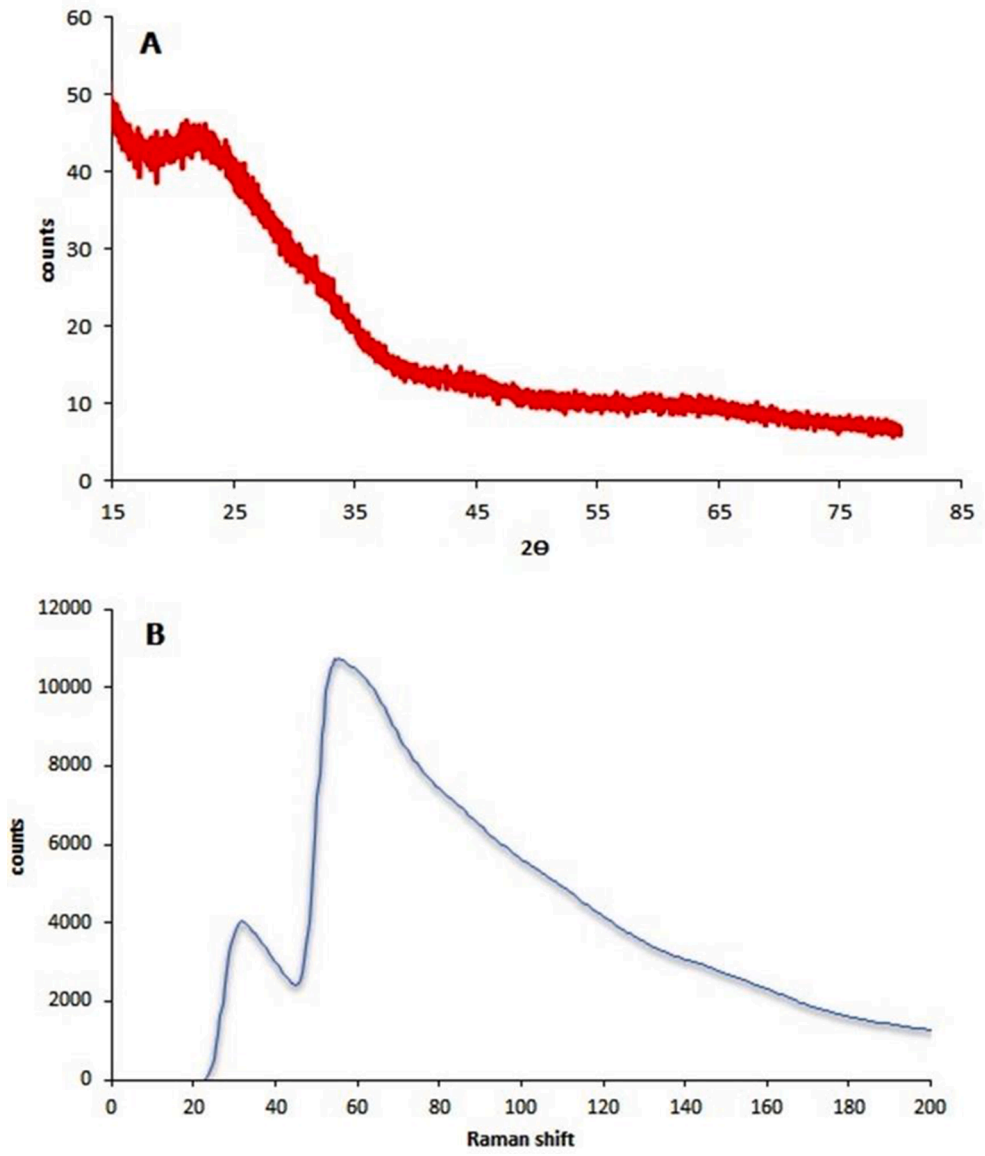

Fig. 2. (A) X-ray Diffraction (XRD) pattern of AgNPs illustrated the amorphous nature of Silver nanoparticles (B) Raman spectra of amorphous AgNPs showed characteristic peaks at 52.1 and 146.5.

measurements. The X-ray source used was Cu Kα radiation with a current of 32 mA and voltage of 41 kV. The 2θ angles ranged from 20 to 70° for Se-NPs and from 35 to 90° for AgNPs with a scan speed of 0.3°/ min. The Raman spectra achieved by a Horiba lab RAM HR evolution spectrometer. The 532 nm edge laser line with Raman shift range from 100 to 1000 cm^{-1} for Se-NPs and AgNPs range from 20 to 200 cm^{-1}, grating (450–850 nm) and ND filter 10% to prevent oxidation of Se-NPs and AgNPs. Acquisition time was 15 secs, accumulations of 4 without spike filter and objective was X100.

2.3.2. Index class

BET method (the Brunauer– Emmett–Teller isotherm) used to determine the specific surface area by pore and surface area analyzer manufacturer by Quantachrome, model of NOVA touch LX2. Sample was degassed at 80 °C for 3 h. under vacuum. DLS and zeta potential achieved by DLS and zeta potential analyzer (Malvern, UK).

2.3.3. Microscopic class

Atomic Force Microscope (AFM) (5600LS, Agilent, USA) was used its 2D and 3D AFM images to determine surface topography of Se-NPs and AgNPs. Firstly, samples were prepared by subjecting samples to ultrasound waves for 15 min, a condition of 50 kHz, at an amplitude of 44% and 0.45 of a cycle (Up 400 s manufacture by Hielscher, German). Finally, created a thin film using Spain coater instrument model Laurell-650Sz at the condition of 700 rpm under vacuum. AFM images and data profile have been done for 200 nm X 200 nm and its zoom 100 nm X 100 nm using contact mode, Al tap, 0.71 In/S speed, I. gain 2 and P. gain 4. Scanning electron microscopy (SEM) instrument have been done to study Se-NPs surface morphology. The SEM images was achieved by Jol 2000, Japan. Transmission electron microscopy (TEM) study was performed by added Se-NPs to deionized water and sonicating for 15 min using ultrasound prop with a 60 kHz, at an amplitude of 41% and 0.41 of a cycle (Up 400 s, Hielscher, German). TEM experiments were achieved using (Jeol, JEM-2100 high-resolution, Japan).

2.4. Statistical analysis

All data are expressed as mean ± SD. The difference between groups was statistically analyzed by GraphPad Prism 6 (La Jolla, CA, USA), using one-way ANOVA followed by Tukey's Kramer Multiple

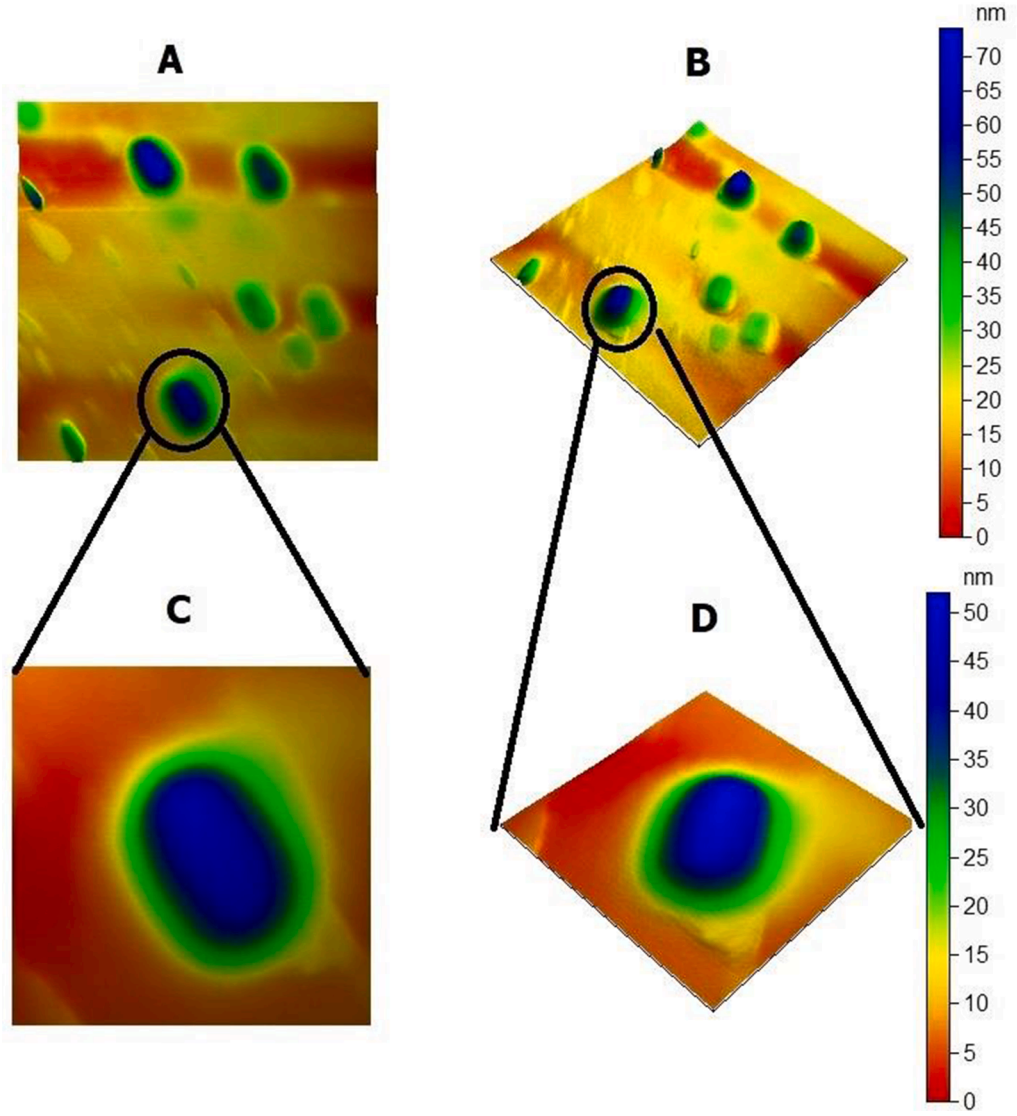

Fig. 3. Atomic Force Microscope (AFM) image of colloidal Se-NPs nanoparticles A) 2D view AFM image of 200 nm X 200 nm size B) 3D view AFM image of 200 nm X 200 nm size C) 2D view AFM image of 100 nm X 100 nm size D) 3D view AFM image of 100 nm X 100 nm size. 2D and 3D AFM images and data showed that colloidal Se-NPs nanoparticles samples have excellent homogenous surface topography. In addition, AFM images illustrated the rode shape (blue) with excellent caping of citrate (green) composed core–shell nanostructure with dramatic shape.

Comparison Test. P-value < 0.05 was considered as significant.

3. Results

3.1. Characterization of silver nanoparticles and selenium nanoparticles

3.1.1. Identification

(XRD) pattern of Se-NPs showed the characteristic peaks for Se-NPs at $2\theta = 23.5°$, 29.6°, 41.3°, 43.5°, 45.3°, 48.2°, 51.7°, 56°, 56.1°, 61°, 61.2°, 65.2°, 68.2 and 68.4° which as shown in Fig. 1B. while XRD pattern of AgNPs illustrated the amorphous nature of Silver nanoparticles as shown in Fig. 2A. These results indicate the high crystallinity of Se-NPs. Concerning the Raman spectrum of colloidal Se-NPs, the characteristic Raman shift peaks was illustrated in Fig. 1A without any shift or contaminated peaks with a very strong sharp peaks at 300 cm-1. While Raman spectra of amorphous AgNPs showed characteristic peaks at 52.1 and 146.5 of vibration AgNPs as illustrated in Fig. 2B.

3.1.2. Microscopic class

2D and 3D AFM images and data showed that colloidal Se-NPs nanoparticles samples have excellent homogenous surface topography. In addition, AFM images illustrated the rode shape (blue) with excellent caping of citrate (green) composed core–shell nanostructure with dramatic shape and structure change where most of literature synthesis spherical Se-NPs and the cap was not recognized as shown in Fig. 3. While for AgNPs as shown in Fig. 4, AFM images showed its spherical shape with very sharp edges and homogenous in size and shape. Scanning Electron Microscope (SEM) and Transmission Electronic Microscope (TEM) results for AgNPs were found in accordance with AFM results as show in Fig. 6. Colloidal Se-NPs nanoparticles have rode core–shell nanostructure with very sharp edge of both core and shell with width size about 30 nm and length about 200 nm. While AgNPs have spherical shape with size range from 15 to 25 nm. Sem image also determined the rode core–shell nanostructure of Se-NPs and spherical shape of AgNPs as shown in Fig. 5..

Index class:

BET surface area measured for Se-NPs and AgNPs was 25.8 m^2/g and 70.1 m^2/g respectively. The Nitrogen adsorption–desorption isotherm curve shows unity IV type isotherms with mesopoues as shown in Fig. 7 for Se-NPs and IV type for AgNPs as shown in Fig. 8. Zeta sizing and potential illustrated in Table 1 and Fig. 7B and 8B, the results showed the very strong stability of Se-NPs and AgNPs in aqueous solution due to its high zeta potential value which confirm the colloidal properties of both of them. The DLS curve for Se-NPs illustrated the presence of two sharp peaks at size about of 50 nm and 200 nm which confirm the presence of two sizes; one for length and other for width of rode

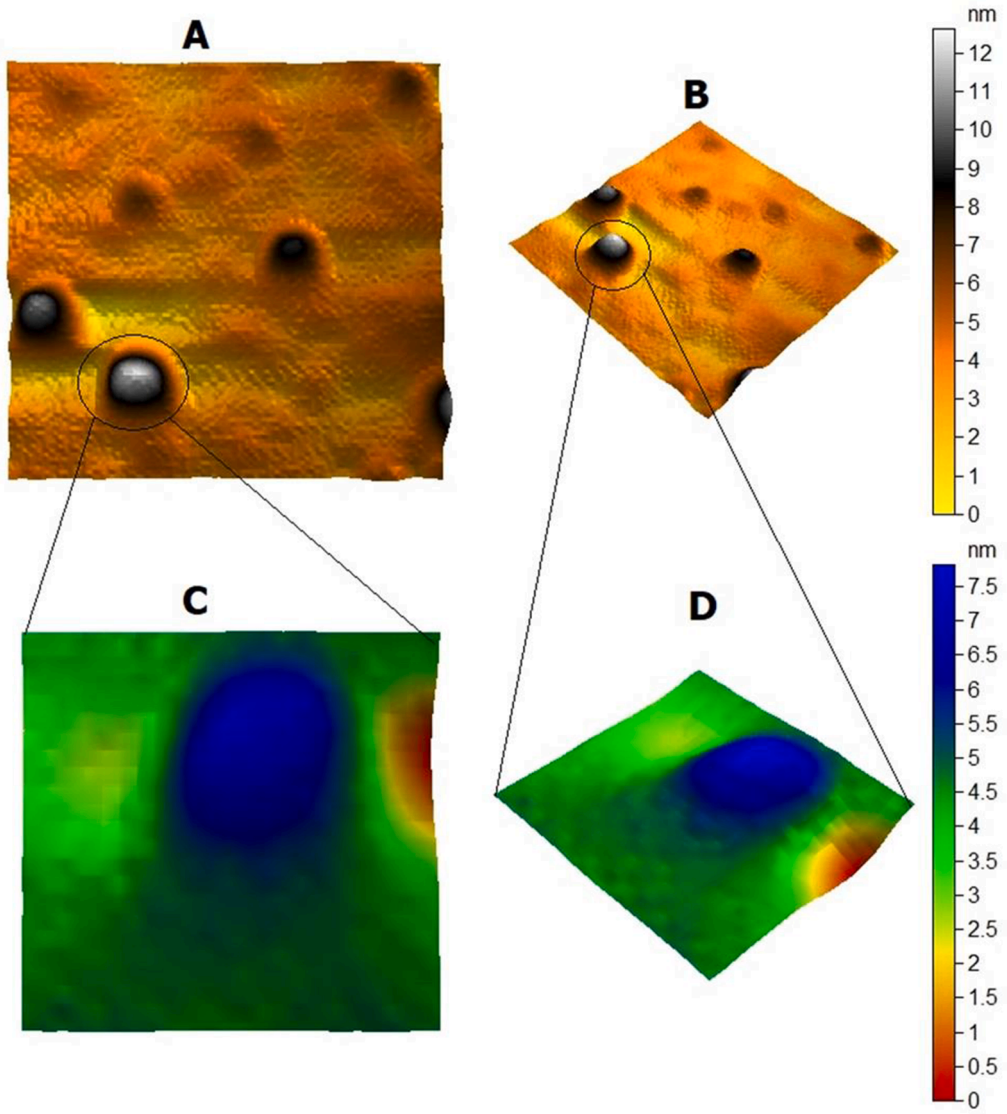

Fig. 4. Atomic Force Microscope (AFM) image of colloidal Silver nanoparticles A) 2D view AFM image of 200 nm X 200 nm size B) 3D view AFM image of 200 nm X 200 nm size C) 2D view AFM image of 100 nm X 100 nm size D) 3D view AFM image of 100 nm X 100 nm size. AFM images showed its spherical shape with very sharp edges and homogenous in size and shape.

core–shell nanostructure as shown in Fig. 7C. While AgNPs curve showed one sharp peak at 15 nm as shown in Fig. 8C.

3.2. Interpretations of AgNPs

3.2.1. AgNPs improved liver function tests

In group treated with Ags (0 to 100 nm), ALT level was ranged from (31: 44 U/L) with the mean equal to (37.5 U/L ± 2.5) showing significant increase compared to normal ones but significant decrease in comparison to LPS groups ($P < 0.05$). Also, in group of Ag with large particle size, ALT level was ranged from (35: 46 U/L) indicating significant increase in comparison to normal group but significantly decreased in comparison to LPS group ($P < 0.05$); while it shows no significant difference in comparison to group of Ag with small particle size. Similarly, AST level was ranged from (19: 22 U/L) with the mean equal to (20.3 U/L ± 0.6) showed significant decrease in comparison to LPS or NAC groups ($P < 0.05$). In NAC + AgL group, AST level showed (19.7 U/L ± 0.6) significant increase in comparison to normal while it causes a significant decrease in AST level in comparison to LPS or NAC group ($P < 0.05$) as shown in Fig. 9 A&B.

3.2.2. Antioxidative and Anti-inflammatory effects of AgNPs

The bacterial infection in LPS group resulted in a 2.6-fold decrease in the lipid peroxidation marker expressed as glutathione (GSH) compared with control liver slices indicating liver damage. Treatment with AgS increased GSH by around 40% and similarly In Ag L group, treatment caused 2-fold increase in GSH level compared to LPS group (Fig. 9 C).

The anti-inflammatory properties of AgNPs in Liver slices were assessed by measuring the IL-6 and TNF-α levels. Treatment with both AgS and AgL resulted in the decrease of the anti-inflammatory IL-6 and the decrease of the pro-inflammatory TNF-α. Upon treatment with AgS, the IL-6 decreased by more than 1.6-folds while AgL decreased it by 1.5-folds. On the other hand, AgS treated group decreased TNF-α by 21% compared to the diseased LPS group while AgL surpassed this to reach 32% decrease in the levels of TNF-α as shown in Fig. 10.

3.2.3. Histopathological and immunohistochemistry assessment

H&E staining revealed significant changes obtained in the histological examination between the control, LPS and treated groups with small and large particles of AgNPs. In the LPS group, the liver tissue shows activation of Kupffer cells and sporadic hepatocytes necrosis while both the AgS and the AgL groups showed slight activation of Kupffer cells and

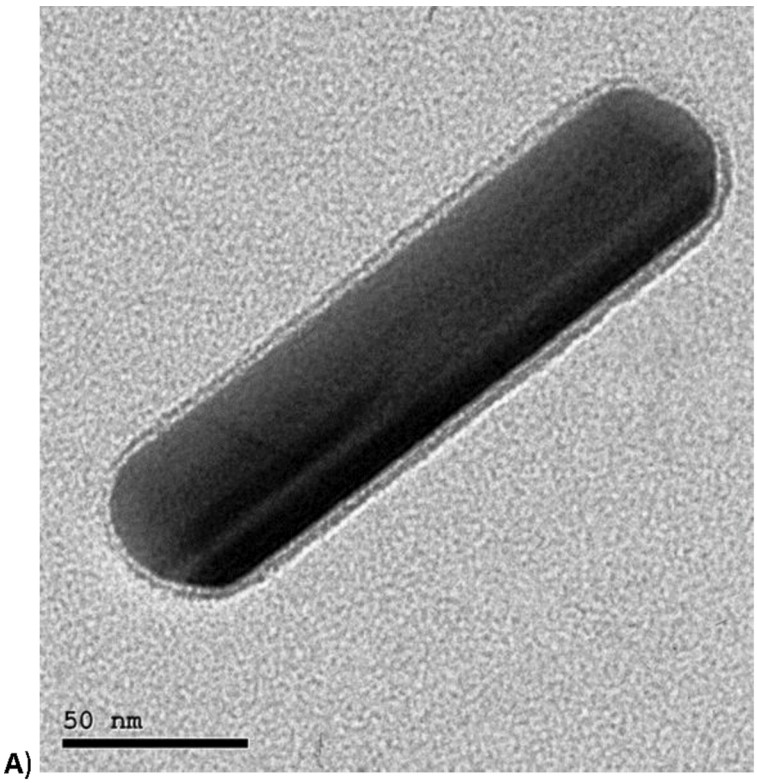

A)

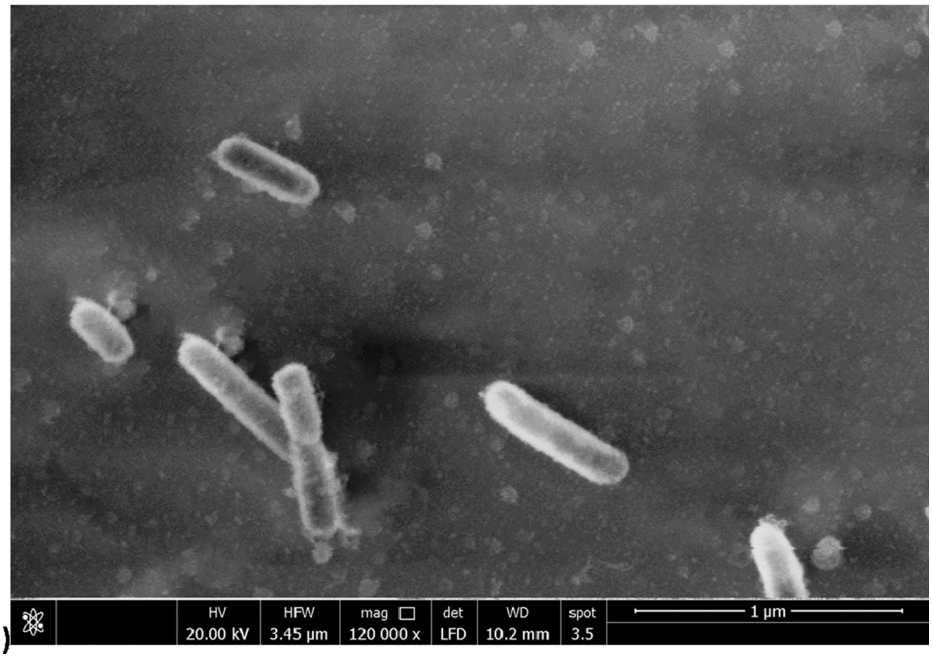

B)

Fig. 5. A) Transmission electron microscopy (TEM) image illustrates the Colloidal Se-NPs nanoparticles have rode core–shell nanostructure with very sharp edge of both core and shell with width size about 30 nm and length about 200 nm and B) Scanning electron microscopy (SEM) image illustrates the rode core–shell nanostructure of Se-NPs.

few necrosis effects of hepatocytes (Fig. 11). Immune expression of CD68 in liver slices is illustrated in Fig. 12. The liver slices of control group showed normal expression of CD68 cells. On contrary, CD68 expression was significantly increased in LPS group compared to the control group. While the AgS and the AgL treated groups exhibited a significant improvement in reduction of CD68 expression in comparison to LPS group.

3.3. Interpretations of SeNPs

3.3.1. SeNPs improved liver function tests and reduced oxidative stress marker

After treatment of HBV-hepG2 cell lines with SeNPs, both ALT (U/L) and AST (U/L) levels were increased by 1.7 and 2.5-folds while the MDA concentration decreased. SeNPs administration enhanced the liver

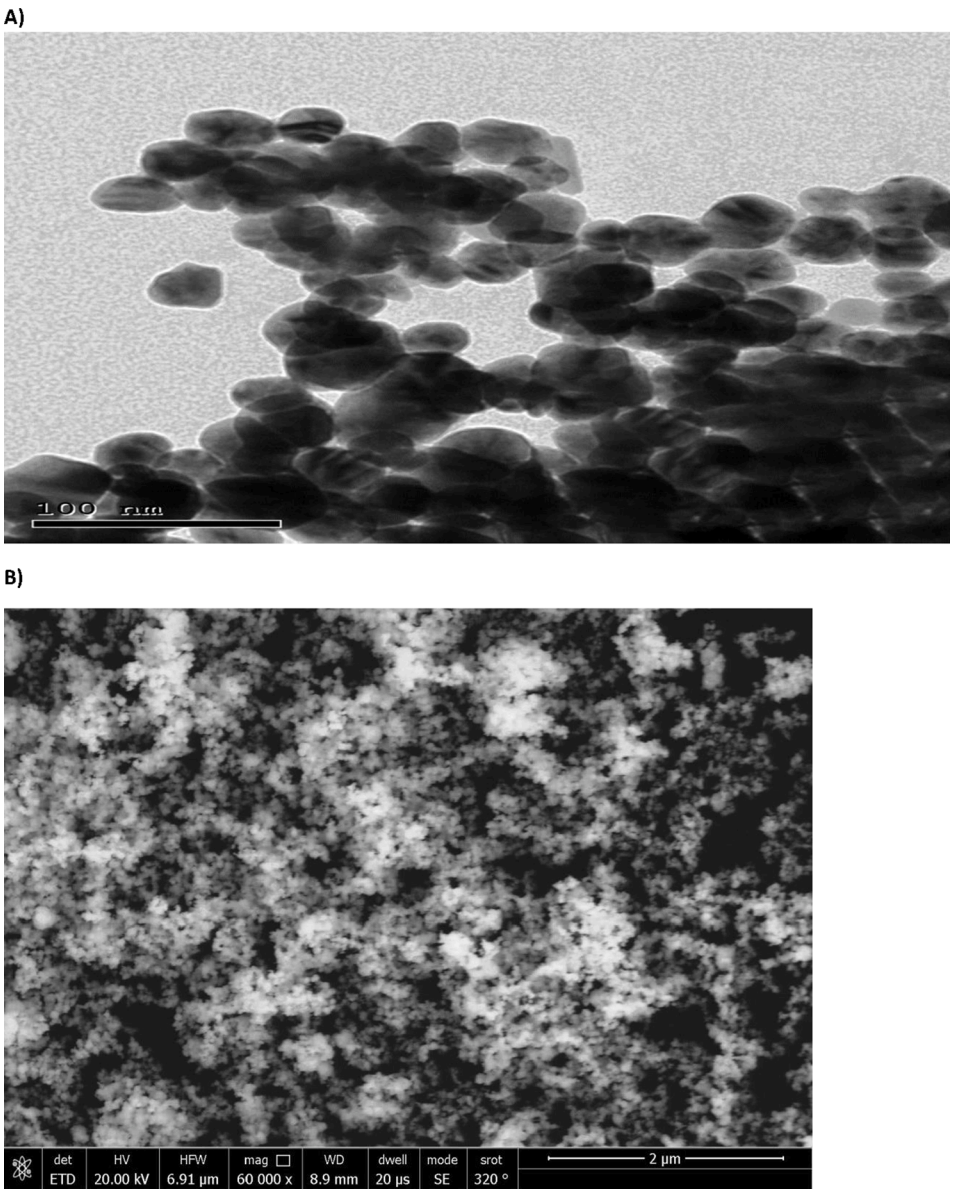

Fig. 6. A) Transmission electron microscopy (TEM) and B) Scanning electron microscopy (SEM) images of AgNPs illustrates the spherical shape of AgNPs with size range from 15 to 25 nm.

function tests and decreased the level of both enzymes as well as decreasing the secretion of MDA by 1.2-fold **(**Table 2**).**

3.3.2. Anti-inflammatory effects of SeNPs in HBV-replicating human HCC cell line HepG2

SeNPs showed 1.3-fold and 1.5 decrease in both proinflammatory markers TNF- α and TGF levels in HepG2 cell lines after administering of SeNPs. These values were decreased significantly after treatment. Additionally, SeNPs decreased the level of IL-8 by 46 % and IL-2 by 43%. Treatment with SeNPs lowered the level of all proinflammatory markers significantly compared to the control group (Fig. 13).

3.3.3. Effects of SeNPs on DNA fragmentation

The effect of the administration of SeNPs on DNA fragmentation in HepG2 cell lines is illustrated in Fig. 14. A significant more than 8-fold increase in the tail length and 3.7-fold increase in tail DNA% (tDNA%) was shown in the HepG2 cell lines infected with HBV. Treatment with SeNPs significantly protected HepG2 cell lines from DNA damage as indicated by a decrease the tDNA% by 17% compared to the diseased group.

4. Discussion

Recently, studies focused on the ability of nanoparticles in drug delivery and targeting, leading to treatment of various liver diseases [13,14]. Consequently, this study investigated the effects of both AgNPs and SeNPs on liver tissue injury due to viral and bacterial causes. The study showed different mechanisms for the effect of AgNPs on liver tissue even at low concentration; either through the particle size of the AgNPs or through the down regulation of secretion of cytokines by hepatic cells, which may lead to HSC activation.

Another evidence was observed in the histological changes including, necrosis and hepatocellular degeneration that were dose dependent. Several studies confirmed that liver is the main target organ for the effect of AgNPs and showed that liver tissue after treatment with AgNPs exposure may be associated with reduction of oxidative stress [15,16]. It is known that oxidative stress is a main mechanism by which silver nanoparticle affect treatment of injured liver tissues [17,18]. In

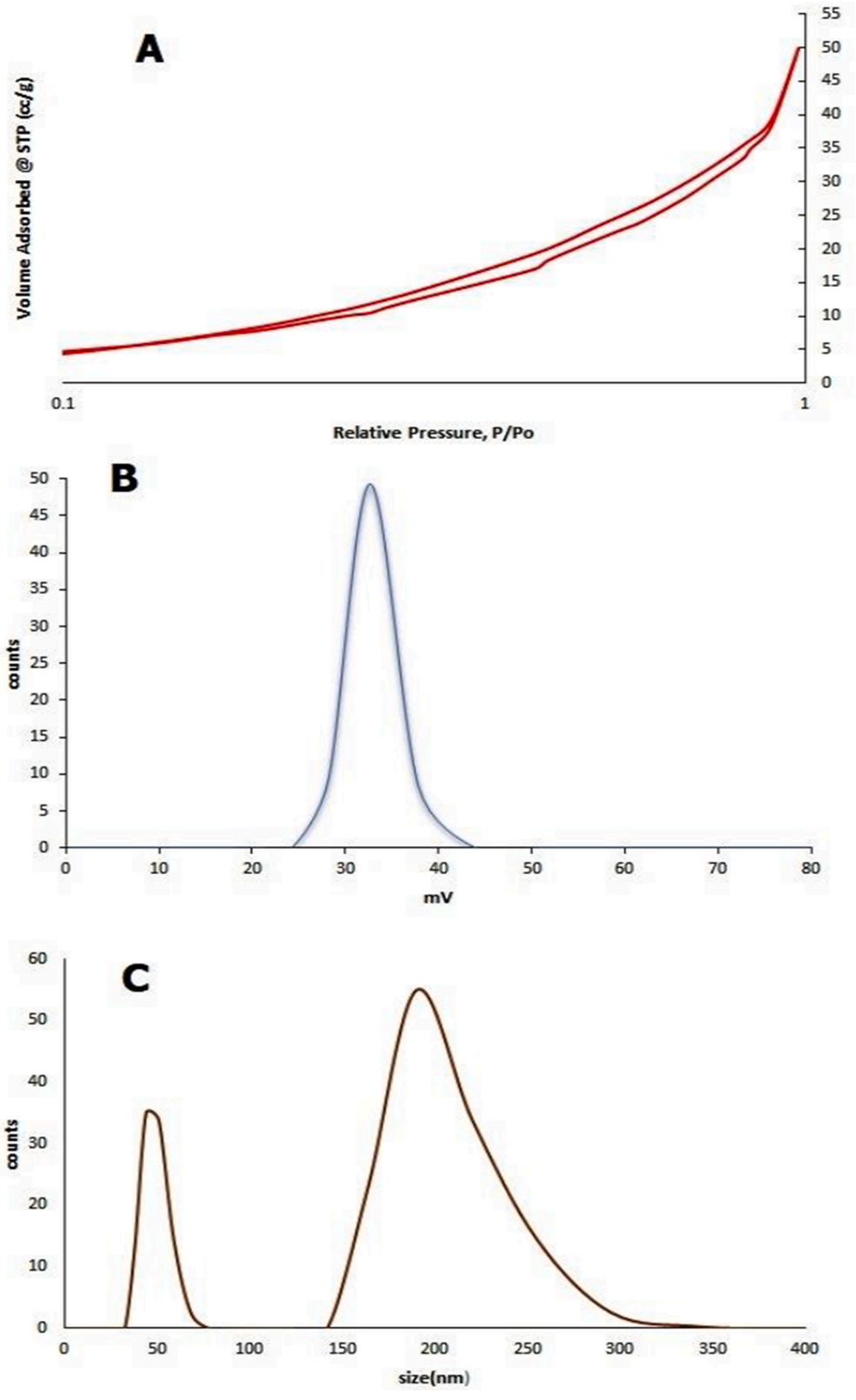

Fig. 7. A) The Nitrogen adsorption–desorption isotherm curve shows unity IV type isotherms with mesopoues Se-NPs B) Zeta sizing and potential of Se-NPs showed the very strong stability of Se-NPs in aqueous solution due to its high zeta potential value which confirm the colloidal properties of both of them. C) The DLS curve for Se-NPs illustrated the presence of two sharp peaks at size about of 50 nm and 200 nm which confirm the presence of two sizes; one for length and other for width of rode core–shell nanostructure.

this study, markers of oxidative stress and inflammatory mediators were measured in the liver tissues. We observed a significant decrease in GSH level and a significant increase in TNF- and IL-6 in hepatocytes. Our study suggests that the ability of AgNPs to cause a significant decline in the inflammatory markers leads to reduce apoptosis through inflammatory and oxidative stress mechanisms.

Several previous studies have focused on the effect of nanoparticle size on cytotoxicity and cellular uptake [19]. In this study, AgNPs of two different sizes classified as small particle size (10 nm and 75 nm) and large particle size (250–300 nm) at different concentrations were included in the treatment of bacterial infected liver slices together with NAC. Activation of HSCs is significant in development of liver disease

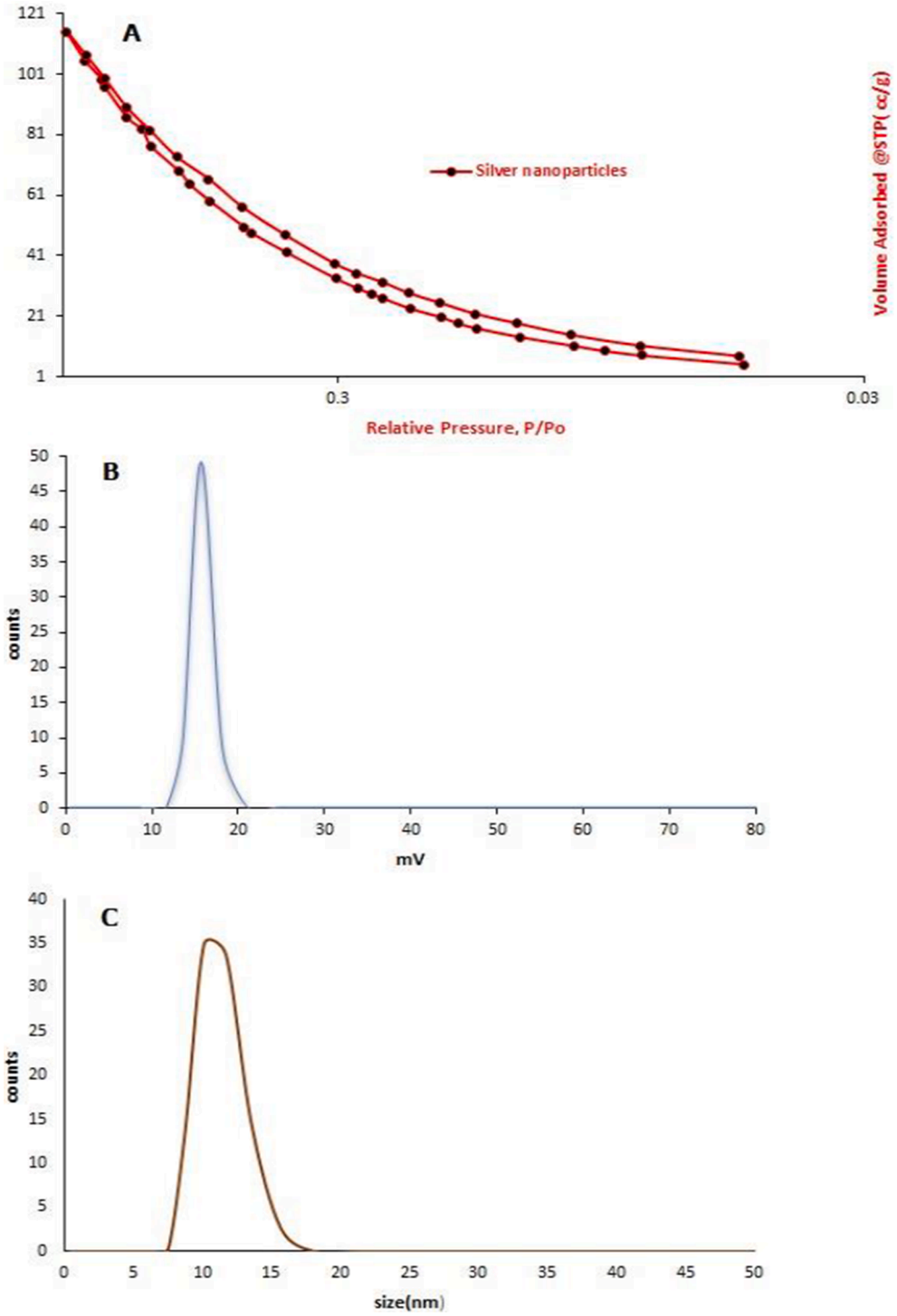

Fig. 8. A) The Nitrogen adsorption–desorption isotherm curve shows unity IV type isotherms with mesopoues of AgNPs B) Zeta sizing and potential of AgNPs showed the very strong stability of AgNPs in aqueous solution due to its high zeta potential value which confirm the colloidal properties of both of them. C) DLS curve of AgNPs showed one sharp peak at 15 nm.

through the secretion of many cytokines. The results of the Elisa assay demonstrated that the anti-inflammatory effects exerted by AgNPs on HSCs are size- and dose-dependent. Larger AgNPs showed significant reduction in TNF- α than the smaller particles, while for the anti-inflammatory marker; IL-6, both small and large particles showed significant reduction in IL-6 compared to the LPS group. According to our study, the other mechanism by which AgNPs can treat the liver bacterial infection occurs through its effects on the up-regulation of antioxidants (GSH) and this was clearly obvious in the groups treated with small and large AgNPs compared to LPS group.

Moreover, AgNPs affected successfully the liver function tests, this was confirmed by the significant decrease of AST and ALT levels in groups treated with NAC together with small and large particles compared with LPS group and group treated with NAC only, which indicate a significant protective role of AgNPs. Therefore, the reducing effects of AgNPs on production of important cytokines as well as liver function tests which was also confirmed by other previous studies may suppress the progression of hepatic fibrosis; however, the detailed

Table 1
Summary of Zeta size and Potential of all silver and selenium nanoparticles samples.

samples	Size (nm)	potential
Se-NPs	45	-32.1
AgNPs	15	-18.9

BET method (the Brunauer– Emmett–Teller isotherm) used to determine the specific surface area by pore and surface area analyzer manufacturer by Quantachrome, model of NOVA touch LX2. Zeta potential achieved by zeta potential analyzer.

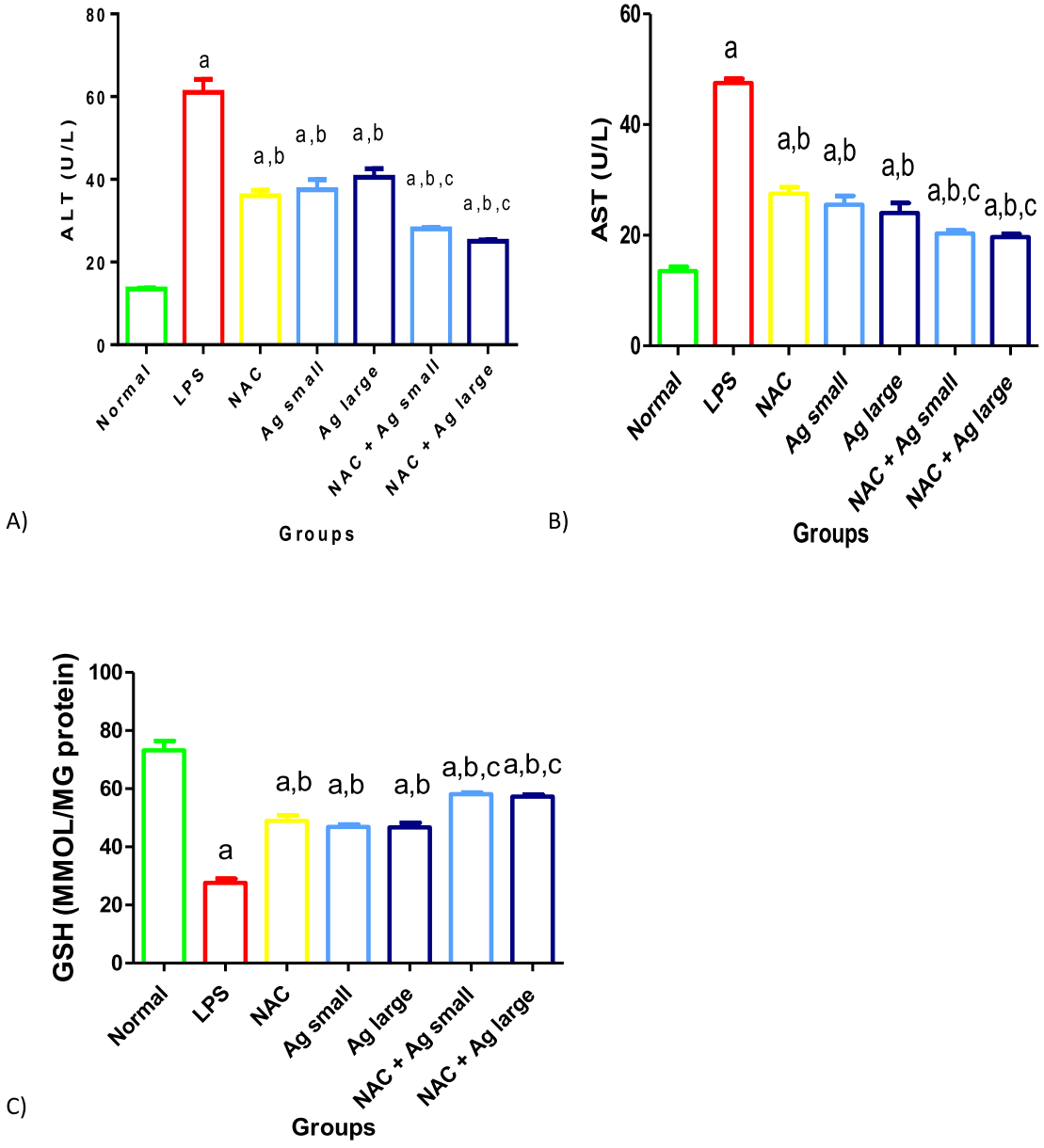

Fig. 9. (A) Effect of treatment with AgNps on ALT levels in the studied groups. (B) Effect of treatment with AgNps on AST levels in the studied groups (C) Effect of treatment with AgNps on GSH levels in the studied groups. Treatment with both small and large Ag nanoparticles significantly decreased liver function tests in comparison with LPS group. The bacterial infection in LPS group resulted in a 2.6-fold decrease in the lipid peroxidation marker expressed as glutathione (GSH) compared with control liver slices indicating liver damage. Each value represents the mean of 6 experiments ± SD. a: significant difference versus the control group; b: significant difference versus the LPS group, c: significant difference versus the NAC group.

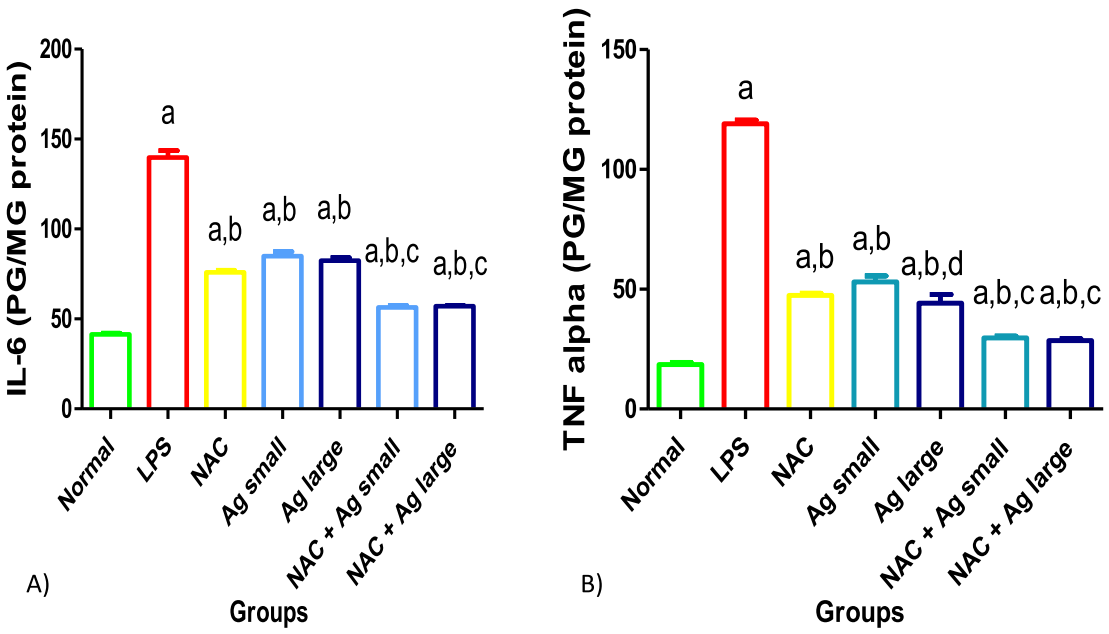

Fig. 10. (A) Effect of treatment with AgNPs on the IL-6 levels in the studied groups. (B) Effect of treatment with AgNPs on the TNF-α levels in the studied groups. Treatment with both AgS and AgL resulted in the decrease of the anti-inflammatory IL-6 and the decrease of the pro-inflammatory TNF-α. Each value represents the mean of 6 experiments ± SD. a: significant difference versus the control group; b: significant difference versus the LPS group, c: significant difference versus the NAC group; d: significance in relation to AgS.

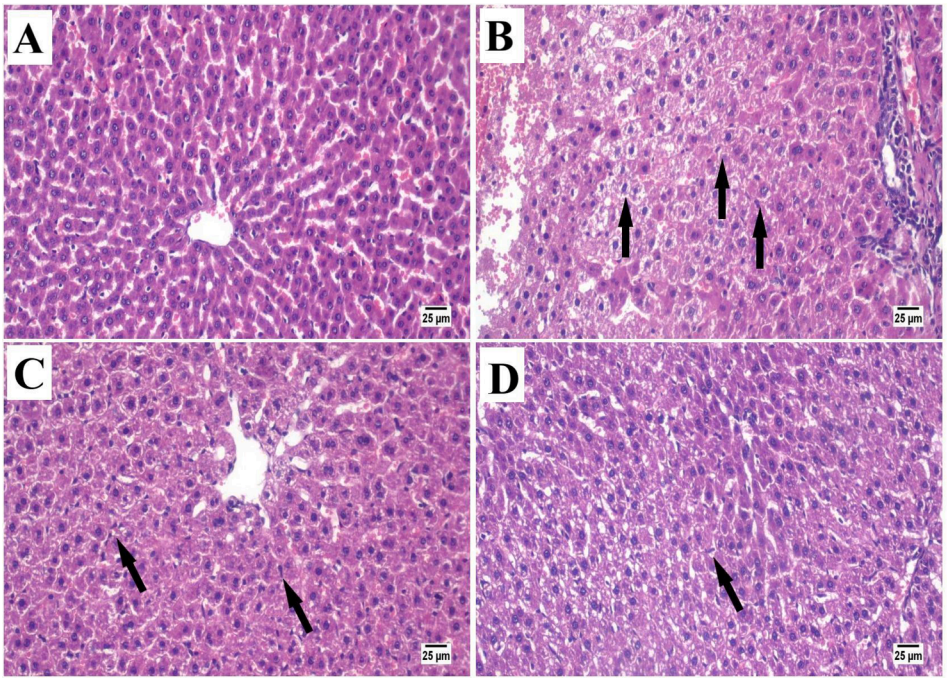

Fig. 11. H&E stain (x400) (A) Liver slices of control group showing no histopathological changes (B) Liver of LPS group showing Kupffer cells activation and necrosis of sporadic hepatocytes. (C) Liver slices treated with AgS showing some Kupffer cells activation and few necrosis of sporadic hepatocytes (D) Liver slices treated with AgL showing slightly Kupffer cells' activation and few necrosis of sporadic hepatocytes.

mechanisms require more studies [20]. The size of AgNPs is highly significant in the cellular uptake by tissues, and thus affecting their bioactivity [21]. The design of nanoparticles for medical applications should take into consideration the particle size to obtain the maximum effect.

There are several causes for chronic liver disease including; alcohol addiction, fatty liver, fibrosis, hepatitis B and C and cirrhosis [22]. Recently SeNPs are considered a potential tool for treatment of cancers due to its chemical protective agent against toxic side effects of anti-cancer drugs [23]. In the present study, the treatment of HBV-replicating human cell line HepG2 with SeNPs showed significant alterations in inflammatory mediators produced by injured liver tissue and DNA fragmentation.

Endocytosis has been proved as an important cellular uptake mechanism for nanoparticles. Many previous studies confirmed that selenium nanoparticles divide into smaller particles under the acidic conditions of

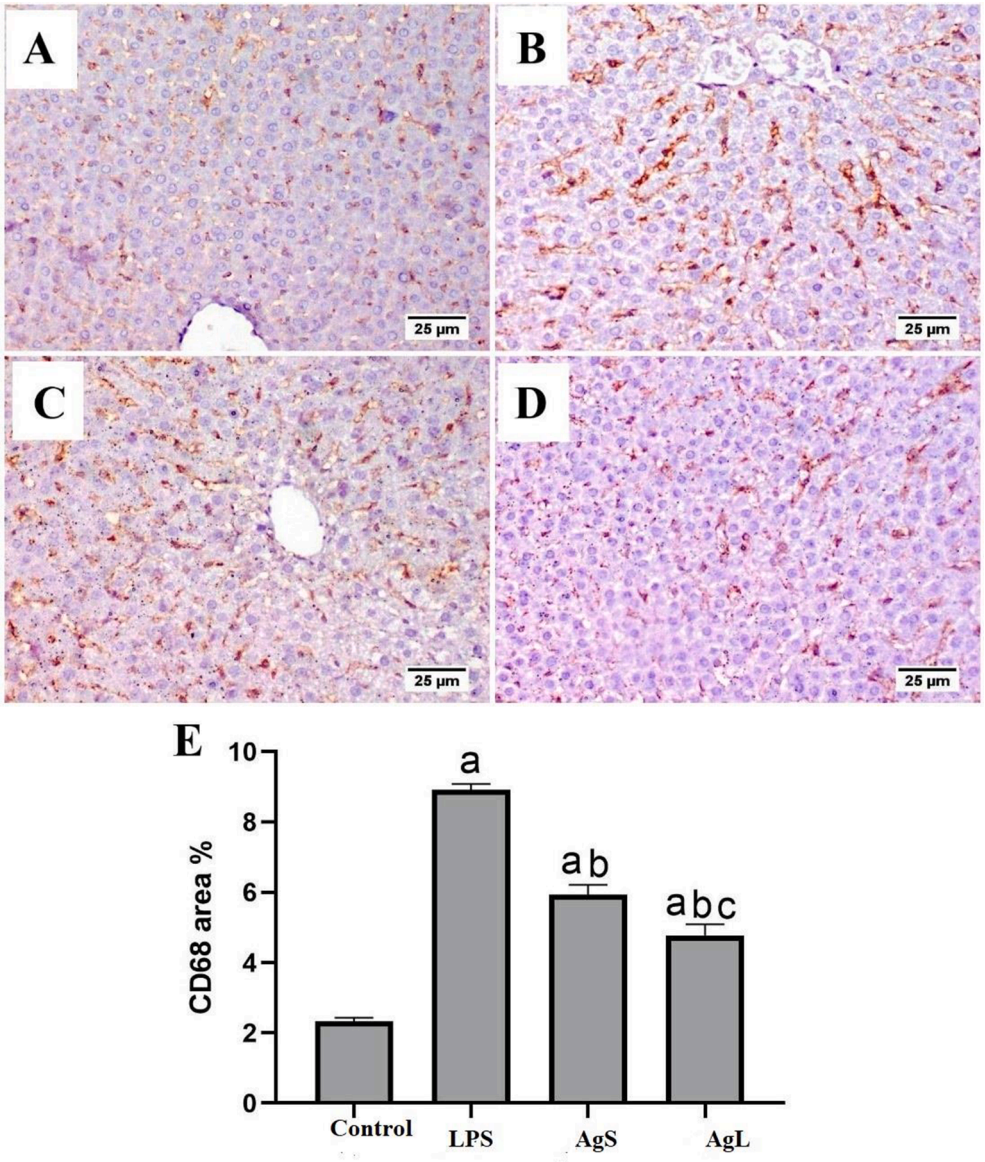

Fig. 12. Immunostaining of CD68 in liver tissue. (A) Liver slices of control group showing normal expression of CD68 cells (B) Liver of LPS group showing a significant increase in CD68 expression (C) Liver slices treated with AgS showed a significant improvement in reduction of CD68 expression and (D) Liver slices treated with AgL showing a greater reduction of CD68 expression compared with other groups. (E) Quantification of CD68 positive cells as area % of expression. Value presented as means ± SE significant difference was considered at $P < 0.05$. a: significant difference versus the control group; b: significant difference versus the LPS group, c: significant difference versus the AgS treated group.

Table 2
Effect of treatment with SeNPs on liver function enzymes and MDA in the control, HBV and HBV-NP groups.

Group	ALT (U/L)	AST (U/L)	MDA (g/dL)
Control	37.59 ± 3.56	38.42 ± 3.59	1.03 ± 0.18
HBV cell line HepG2 (HBV)	75.38 [a] ± 5.28	85.1 [a] ± 16.12	1.4 [a] ± 0.24
HBV cell line HepG2 treated with SeNPs (HBV-NP)	53.8 [a] ± 3.89	57.11 [a] ± 4.49	1.2 [a] ± 0.28

Statistical analysis was performed using one-way ANOVA followed by Tukey's multiple comparison post hoc test; a: significant difference versus the control group.

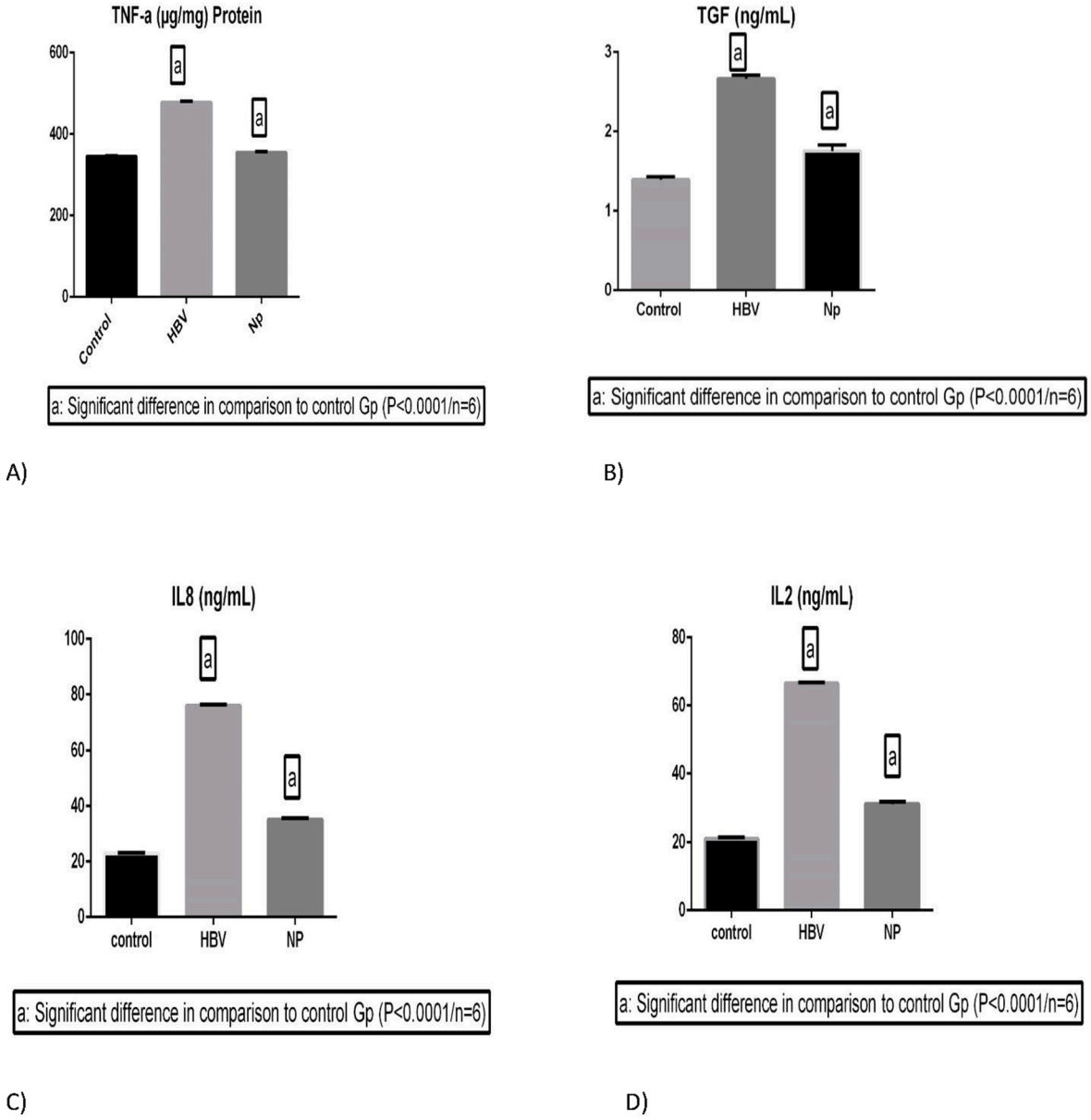

Fig. 13. (A) Effect of treatment with SeNPs on the TNF-α levels in the control, HepG2 cell lines and SeNPs treated groups. (B) Effect of treatment with SeNPs on the TGF levels in the control, HepG2 cell lines and SeNPs treated groups. SeNPs showed 1.3-fold and 1.5 decrease in both proinflammatory markers TNF- α and TGF levels in HepG2 cell lines after administering of SeNPs. (C) Effect of treatment with SeNPs on the IL-8 levels in the control, HepG2 cell lines and SeNPs treated groups. (D) Effect of treatment with SeNPs on the IL-2 levels in the control, HepG2 cell lines and SeNPs treated groups. Additionally, SeNPs decreased the level of IL-8 by 46 % and IL-2 by 43%. Each value represents the mean of 6 experiments ± SD. a: significant difference versus the control group.

the lysosomes, which helps the metabolism of SeNPs and the release of the loaded drugs [24].

Lipid peroxidation markers are products of oxidation and reduction process, including highly toxic compounds [25]. These markers are considered to be a significant factor in cancer prevalence and recurrence. In addition, many studies have shown that alterations in lipid oxidation and inflammatory markers level in cells affect cell apoptosis and in turn could be used in treatment [26].

Our results agree with another study conducted by [27] who suggested that this injury is caused due to increase in the oxidative stress process in liver, and this was clearly obvious in our study which showed significant reduction in MDA levels in treated group with SeNPs compared to HepG2 cell lines. Moreover, our results were also confirmed by a recent study [24] which found that HBV causes inflammation and chronic liver injury which affects the damage of DNA, our current findings showed significant decrease in the inflammatory markers; TNF- α, TGF, IL-6 and IL-2 in the HepG2 cell lines treated with SeNPs compared to HBV-HepG2 cell lines. Additionally, the increase in DNA damage in HBV cell lines which may be due to the release of free radicals including nitric oxide reactive species (NOS) and reactive oxygen species (ROS) which leads to liver injury [28]. These ROS led to inflammatory responses, necrosis of liver cells and fibrogenesis [29].

Our current results of comet assay showed that the treatment of HBV-cell lines with SeNPs caused significant decrease in DNA damage compared to HBV-cell lines, these results were reported also by another study [30]. Taken into consideration, previous studies have shown that SeNPs has a significant therapeutic action for several diseases such as inflammation, cancer, and viral infection [31,32], for this reason, this nano system is drawing great attention in the field of therapy due to its higher stability, antiviral activity, anti-inflammatory activity and low toxicity compared to other nanoparticles.

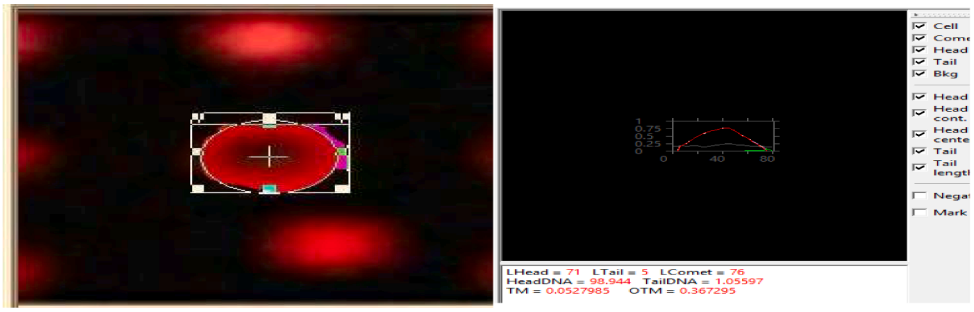

A) Comets from hepatocytes of control group

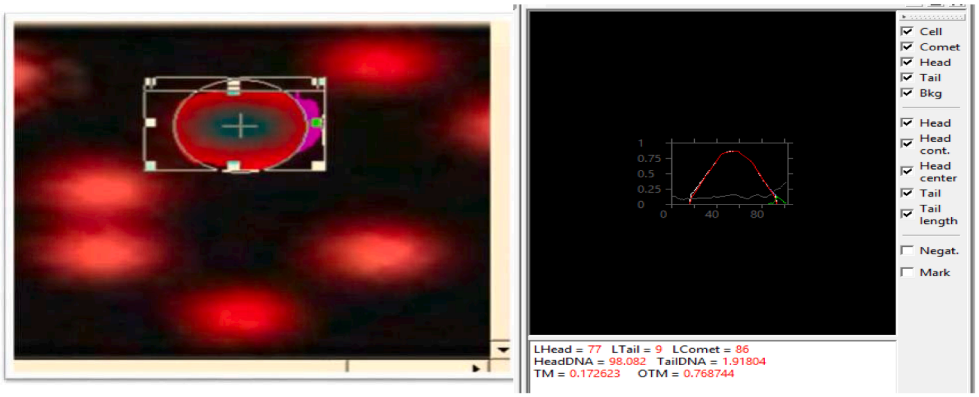

B) Comets from hepatocytes of HBV group

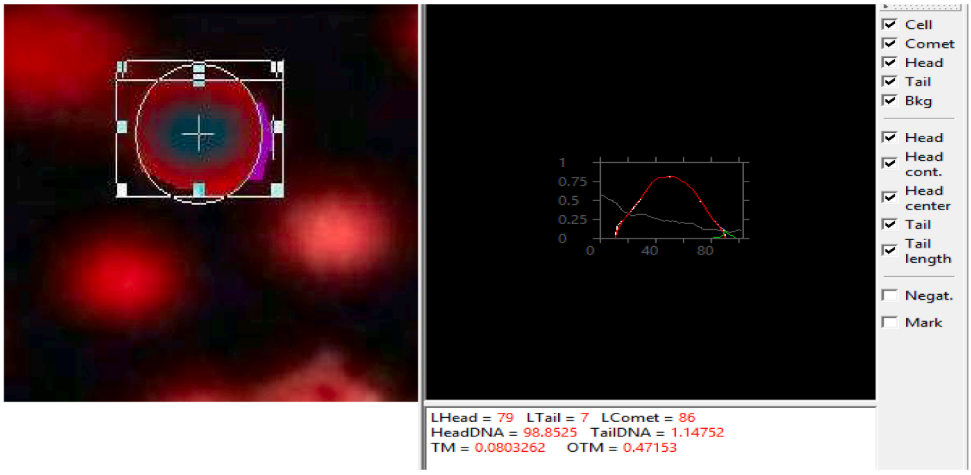

c) Comets from hepatocytes treated with SeNPs group

Fig. 14. Effect of treatment with SeNPs on DNA fragmentation. Comets from hepatocytes: a: control, b: HBV, c: SeNPs treated. Treatment with SeNPs significantly protected HepG2 cell lines from DNA damage as indicated by a decrease in the tDNA% by 17% compared to the HBV group.

5. Conclusion

In view of the present study, the efficacy of AgNPs was investigated by different biochemical approaches and it was particle dose and particle-dependent. The biochemical alterations in the inflammatory and oxidative stress markers may be an indication of the anti-oxidant activity and the inhibitory activity of proliferation of injured cells caused by AgNPs in liver tissue. On the other hand, SeNPs played a potential role in reducing DNA damage as well as reduction of several cytokines in HBV-cell lines showing its greater effect as anti-inflammatory and antiviral nanoparticle in comparison with AgNPs. Taken together, both nanoparticles might be an innovative approach for treatment of viral and bacterial liver infection, however more studies are needed to support the use of AgNPs and SeNPs for human disease treatment and prevention.

Ethical approval: The study protocol was approved by the Ethics Committee of the Faculty of Pharmacy, MSA University, Ethics Committee (**code: PH8/EC8/2019F).**

Consent to participate: I understand that all information I provide for this study will be treated confidentially.

Consent for publication.

The signed Consent ensures that the Publisher has the Author's permission to publish the relevant Contribution.

Authors' contributions: SG and SH participated in the study design, practical work especially the molecular biology as well as interpretation of data and manuscript preparation. SM and DA participated in practical work, interpretation of data and manuscript preparation. All authors read and approved the manuscript and all data were generated in-house

and that no paper mill was used.

Funding: This research did not receive any specific grant from funding agencies in the public, commercial, or not-for-profit sectors.

Competing interest: The authors declare that they have no conflict of interest.

Availability of data and materials: All data generated or analyzed during this study are included in this published article.

Declaration of Competing Interest

The authors declare that they have no known competing financial interests or personal relationships that could have appeared to influence the work reported in this paper.

References

[1] P.V. AshaRani, G. Low Kah Mun, M.P. Hande, S. Valiyaveettil, Low Kah Mun G, Hande MP and Valiyaveettil S: Cytotoxicity and genotoxicity of silver nanoparticles in human cells, ACS Nano. 3 (2) (2009) 279–290.
[2] X. Xu, Q. Yang, J. Bai, T. Lu, Y. Li, X. Jing, Fabrication of biodegradable electrospun poly(L-lactide-co-glycolide) fibers with antimicrobial nanosilver particles, J Nanosci Nanotechno. 8 (10) (2008) 5066–5070.
[3] L. Lu, R.-Y. Sun, R. Chen, C.-K. Hui, C.-M. Ho, J.M. Luk, G.KK. Lau, C.-M. Che, Silver nanoparticles inhibit hepatitis B virus replication, Antivir Ther. 13 (2) (2008) 253–262.
[4] A. Schroeder, D.A. Heller, M.M. Winslow, J.E. Dahlman, G.W. Pratt, R. Langer, T. Jacks, D.G. Anderson, Treating metastatic cancer with nanotechnology, Nat Rev Cancer. 12 (1) (2012) 39–50.
[5] Y. Huang, Y. Luo, J. Zheng, T. Chen, ACS Appl. Mater. Interfaces 6 (2014) 19217–19228.
[6] P. Tran, T. Webster, Int. J. Nanomed. 6 (2011) 1553–1558.
[7] T. Liu, L. Zeng, W. Jiang, Y. Fu, W. Zheng, T. Chen, Nanomedicine 11 (2015) 947–958.
[8] O. Choi, Z. Hu, Size dependent and reactive oxygen species related nanosilver toxicity to nitrifying bacteria, Environmental Science and Technology 42 (12) (2008) 4583–4588.
[9] J.T. Rotruck, A.L. Pope, H.E. Ganther, et al., Selenium: Biochemical role as a component of glatathione peroxidase, Science (80-) 179 (1973) 588–590.
[10] Suvarna K S, Layton C BJ (2018) Bancroft's theory and practice of histological techniques (Eighth Edition).
[11] S. Ismail, G. Mohamed, A. Amer, M. Amer, Comparative Killing Activity of Different Nanoparticles and Nanocomposites Based on Dermanyssus gallinae, Nano Biomed. Eng. 12 (4) (2020) 338–350.
[12] J.A. Buege, S.D. Aust, Microsomal Lipid Peroxidation, Methods Enzymol 52 (1978) 302–310.
[13] P. Suchithra, G. Reju, J. Myeong, Y. Yong, Nanoparticles for the treatment of liver fibrosis, Int J Nanomedicine. 12 (2017) 6997–7006.
[14] H.H. Lara, N.V. Ayala-Nuñez, L. Ixtepan-Turrent, C. Rodriguez-Padilla, Mode of antiviral action of silver nanoparticles against HIV-1, J Nanobiotechnology. 8 (1) (2010) 1, https://doi.org/10.1186/1477-3155-8-1.
[15] Y. Wu, Q. Zhou, Silver nanoparticles cause oxidative damage and histological changes in medaka (Oryzias latipes) after 14 days of exposure, Environmental Toxicology and Chemistry 32 (1) (2013) 165–173.
[16] J.E. Choi, S. Kim, J.H. Ahn, P. Youn, J.S. Kang, K. Park, J. Yi, D.Y. Ryu, Induction of oxidative stress and apoptosis by silver nanoparticles in the liver of adult zebrafish, Aquatic Toxicol. 100 (2010) 151–159.
[17] A. Nel, T. Xia, L. Mädler, N. Li, Toxic Potential of Materials at the Nanolevel, Science 311 (5761) (2006) 622–627.
[18] Y.e. Liu, W. Guan, G. Ren, Z. Yang, The possible mechanism of silver nanoparticle impact on hippocampal synaptic plasticity and spatial cognition in rats, Toxicol. Lett. 209 (3) (2012) 227–231.
[19] Y. Yuan, C. Liu, J. Qian, J. Wang, Y. Zhang, Size-mediated cytotoxicity and apoptosis of hydroxyapatite nanoparticles in human hepatoma HepG2 cells, Biomaterials. 31 (4) (2010) 730–740.
[20] M.A.K. Abdelhalim, B.M. Jarrar, Gold nanoparticles induced cloudy swelling to hydropic degeneration, cytoplasmic hyaline vacuolation, polymorphism, binucleation, karyopyknosis, karyolysis, karyorrhexis and necrosis in the liver, Lipids Health Dis 10 (1) (2011) 166, https://doi.org/10.1186/1476-511X-10-166.
[21] V. Purohit, D. Russo, Cellular and molecular mechanisms of alcoholic hepatitis, Alcohol. 27 (1) (2002) 3–6.
[22] Y. Li, X. Tian, Z. Lu, C. Yang, G. Yang, X. Zhou, H. Yao, Z. Zhu, Z. Xi, X. Yang, Mechanism for alpha-MnO2 nanowire-induced cytotoxicity in Hela cells, J Nanosci Nanotechnol. 10 (2010) 397–404.
[23] E. Karavelioglu, M.G. Boyaci, N. Simsek, M.A. Sonmez, R. Koc, M. Karademir, M. Guven, O. Eser, Selenium protects cerebral cells by cisplatin induced neurotoxicity, Acta Cirúrgica Brasileira. 30 (6) (2015) 394–400.
[24] P. Gupta, M.P. Bansal, A. Koul, Lycopene modulates initiation of N-nitrosodiethylamine induced hepatocarcinogenesis: studies on chromosomal abnormalities, membrane fluidity and antioxidant defense system, Chem. Biol. Interact. 206 (2) (2013) 364–374.
[25] B. Zhou, Y. Huang, F. Yang, W. Zheng, T. Chen, Chem.–Asian J. 11 (2016) 1008–1009.
[26] J. Su, H. Lai, J. Chen, L. Li, Y.-S. Wong, T. Chen, X. Li, PLoS One 8 (2013), e63502.
[27] K.A. Amin, K.S. Hashem, F.S. Alshehri, S.T. Awad, M.S. Hassan, Antioxidant and Hepatoprotective Efficiency of Selenium Nanoparticles Against Acetaminophen-Induced Hepatic Damage, Biological Trace Element Research. 175 (1) (2017) 136–145.
[28] M. Lesnichaya, E. Karpova, B. Sukhov, Effect of high dose of selenium nanoparticles on antioxidant system and biochemical profile of rats in correction of carbon tetrachloride-induced toxic damage of liver, Cell. Colloids Surf B Biointerfaces. 197 (2021) 111381, https://doi.org/10.1016/j.colsurfb.2020.111381.
[29] K. Bai, B. Hong, J. He, W. Huang, Antioxidant Capacity and Hepatoprotective Role of Chitosan-Stabilized Selenium Nanoparticles in Concanavalin A-Induced Liver Injury in Mice, Nutrients 12 (3) (2020) 857, https://doi.org/10.3390/nu12030857.
[30] A.H. Abd El-Rahim, O.M. Abd-Elmoneim, N.A. Hafiz, Assessment of Antigenotoxic Effect of Nanoselenium and Metformin on Diabetic Rats, Jordan J. Biol. Sci. 10 (2017) 159–165.
[31] J. Feng, C. Guo, Y. Zhu, L. Pang, Z. Yang, Y. Zou, X. Zheng, Int. J. Clin. Exp. Med. 7 (2014) 4063.
[32] R. Huang, C. Chen, H. Huang, C. Chang, C. Chen, C. Chang, M. Hsieh, Planta Med. 66 (2000) 694–698.